TEMPORAL ERROR ESTIMATION AND ADAPTIVE TIME STEP CONTROL IN UNSTEADY FLOW SIMULATIONS

KATHRIN KOŽULOVIĆ, GRAHAM ASHCROFT[*]

Institute of Propulsion Technology, German Aerospace Center (DLR)
Linder Höhe, 51147 Cologne, Germany, http://www.dlr.de/at/
Email: kathrin.kozulovic@dlr.de, graham.ashcroft@dlr.de

Key words: Unsteady Flow, Time Accurate, Runge-Kutta, High Order, Adaptive Time Stepping, Error Estimation

Abstract. An important factor to control the accuracy of unsteady simulations is the estimation of a numerical scheme's temporal errors. This error estimation can be used to control the time step size, which in turn is beneficial either to achieve a simulation with a prescribed accuracy or to reduce the simulation time by increasing the time step size. The latter procedure is of special interest, since it allows considerable simulation acceleration at the same accuracy as a method with fixed time step size. Furthermore, the adaptive time stepping technique may be considered as a more user-friendly method, since the user does not have to estimate the time step size a-priori and the numerical error a-posteriori, but simply prescribes the error tolerance, and the method automatically adapts to this prescription. In this paper, six explicit first stage, singly diagonal implicit Runge-Kutta (ESDIRK) methods together with different error estimators and corresponding time step adaption have been applied to two generic and one realistic unsteady test cases.

1 INTRODUCTION

Unsteadiness is an essential feature in many kinds of flow, e.g. turbulent boundary layers, turbomachinery, maneuvering, etc. Hence corresponding scientific and engineering investigations largely depend on efficient methods for the numerical computation of time-dependent flow. In this context accurate and robust time-integration schemes are required.

To avoid the time step size restrictions of explicit methods implicit time-integration schemes are commonly employed in the numerical simulation of unsteady flow phenomena. As adaptive time step control is difficult to implement with the popular implicit Backward Differentiation Formulas, within this paper embedded Runge-Kutta methods are used for time-integration and error estimation. These schemes are easy to implement with variable time stepping while the computational costs to evaluate errors estimates are marginal. The excellent stability properties and flexibility of implicit Runge-Kutta

schemes (IRK) above second-order are demonstrated in the context of turbomachinery flows and aerodynamic noise generation [1].

The main focus of this paper is to investigate and assess the error estimation properties of several embedded IRK methods and their efficiency in the context of adaptive time step control. For this purpose error estimators of second-, third- and fourth-order accuracy which are embedded in IRK methods of third- and fourth-order are considered.

The paper is organized as follows. In Section 2 the flow solver used in this work is first briefly described. The IRK methods investigated and their implementation are then discussed in Section 3. The basic properties of methods are then investigated and demonstrated using two academic problems in Section 6. Finally, the results of the investigation are summarized in Section 7.

2   FLOW SOLVER

The high-order accurate time-discretization schemes are investigated in the present work using the CFD code TRACE [2], [3]. TRACE (Turbomachinery Research Aerodynamic Computational Environment) is a parallel Navier-Stokes flow solver for structured and unstructured grids that has been developed at DLR's Institute of Propulsion Technology in Cologne to model and investigate turbomachinery flows. The code solves the compressible Navier-Stokes equations in the relative frame of reference using a multi-block approach. The governing equations are discretized in generalized coordinates about the cell centers using the finite-volume method.

Upwind-biased spatial differencing in conjunction with Roe's flux-difference-splitting method is used to evaluate the inviscid fluxes, with limiters used to obtain smooth solutions in the vicinity of shocks. Viscous terms are discretized using second-order accurate central differences. Turbulence modeling is effected by a $k - \omega$ two-equation approach with turbomachinery-specific extensions.

For the present work it is sufficient to note that following the discretization of the spatial operators in the Navier-Stokes equations the following system of ordinary differential equations (ODE's) is obtained

$$\frac{d\mathbf{U}}{dt} = \mathbf{R}(t, \mathbf{U}(t)) \tag{1}$$

where $\mathbf{U}$ is the vector of conservative variables and t denotes the physical time.

3   IMPLICIT RUNGE-KUTTA METHODS

To avoid the time step size restrictions of explicit methods implicit time-integration schemes are commonly employed in the numerical simulation of unsteady flow phenomena. Although combinations are conceivable, most implicit methods can in general be classified as either multi-step or multi-stage. Both classes of scheme have advantages and disadvantages. Multi-step methods are generally efficient because they solve only one

non-linear set of equations per time step. They are, however, not self-starting, are difficult to use with variable time steps and are not A-stable beyond second-order temporal accuracy. Multi-stage implicit Runge-Kutta schemes on the other hand are self-starting, easy to implement with variable time stepping and can be designed to be A- and L-stable. They do, however, require multiple nonlinear systems to be solved per time step.

As higher-order accurate methods are generally considered to be more efficient than their lower-order counterparts, the excellent stability properties and flexibility of IRK schemes at accuracies above second-order motivates their use in the simulation of time-dependent flow phenomena.

The general form of an s-stage implicit Runge-Kutta scheme applied to Eqn. 1 is

$$\mathbf{W}^i \quad = \quad \mathbf{U}^n + \Delta t \sum_{j=1}^{s} a_{ij} \mathbf{R}(t_n + c_j \Delta t, \mathbf{W}^j), \quad i = 1, \ldots, s \tag{2}$$

$$\mathbf{U}^{n+1} \quad = \quad \mathbf{U}^n + \Delta t \sum_{j=1}^{s} b_j \mathbf{R}(t_n + c_j \Delta t, \mathbf{W}^j) \tag{3}$$

where the superscripts n and $n+1$ denote the time levels at the beginning and end of the current time step, and the superscripts i and j refer to the stage values within the current time-step. The values a_{ij} and b_j denote the Butcher coefficients of the scheme. In this paper several Explicit first stage, Singly Diagonal Implicit Runge-Kutta (ESDIRK) schemes for the numerical integration of the compressible Navier-Stokes equations are considered. This type of numerical schemes allows for embedded error estimation using two methods with different orders of accuracy $q = p \pm 1$, with q as order of the scheme and p the order of the embedded scheme, respectively. Based on this error estimation an adaptive time stepping is done using different controller types. The Butcher tableau for these schemes takes the form

Table 1: Generic Butcher tableau of a four-stage ESDIRK with embedded error estimation

	$c_1 = 0$	0	0	0	0
	c_2	a_{21}	γ	0	0
	c_3	a_{31}	a_{32}	γ	0
	$c_4 = 1$	b_1	b_2	b_3	γ
order of accuracy	q	b_1	b_2	b_3	γ
order of accuracy	$p \pm 1$	$\hat{b_1}$	$\hat{b_2}$	$\hat{b_3}$	$\hat{b_4}$

where c_i denotes the time in the time interval $t_n \rightarrow t_n + \Delta t$ at which the intermediate stage is evaluated. Diagonally implicit schemes are characterized by a lower triangular form of the coefficient table. Each stage of the scheme therefore depends only upon previously solved stages and the system may thus be solved in s successive steps. Singly diagonal schemes use the same diagonal coefficient γ for each stage. The first stage is

3

explicit ($a_{1j} = 0$), which ensures the stages are at least second-order accurate, and the last stage coefficients are such that $a_{ij} = b_j, j = 1, \ldots, s$ which avoids the need to solve Eqn. 3, as the solution of the final stage $\mathbf{W}^s$ is also the solution at the next time step $\mathbf{U}^{n+1}$. The embedded method with $\hat{b}$ depends only on linear combinations of already present stage values $\mathbf{W}^i$.

The ESDIRK methods investigated in this work are given in Tables 2- 5. The first two schemes are the four-stage, third-order accurate ESDIRK methods proposed by Alexander [4] with second- and fourth-order error estimators, respectively.

Table 2: Alexander 3(2/4): Four-stage, 3rd-order ESDIRK method with embedded 2nd- or 4th-order scheme

$$
\begin{array}{c|cccc}
0 & 0 & & & \\
2\gamma & \gamma & \gamma & & \\
c_3 & c_3 - a_{32} - \gamma & a_{32} & \gamma & \\
1 & b_1 & b_2 & b_3 & \gamma \\
\hline
& b_1 & b_2 & b_3 & \gamma \\
& \hat{b}_1 & \hat{b}_2 & \hat{b}_3 & \hat{b}_4
\end{array}
$$

$$a_{32} = \frac{-c_3(c_3 - 2\gamma)}{4\gamma},$$
$$b_1 = \frac{-18\gamma c_3 + 12\gamma^2 c_3 + 3c_3 + 12\gamma - 12\gamma^2 - 2}{12\gamma c_3},$$
$$b_2 = \frac{2 - 3c_3 + 6\gamma c_3 - 6\gamma}{12\gamma(2\gamma - c_3)},$$
$$b_3 = \frac{6\gamma^2 + 1 - 6\gamma}{3c_3(c_3 - 2\gamma)}$$

$$\gamma = 0.435866521508$$

A second-order error estimation results from $c_3 = \frac{1}{2} + \frac{\gamma}{4}$. Choosing $\delta b_3 = 0.096$ and $\delta b_4 = -0.284$ the weights for the error-estimator are $\hat{b}_1 = b_1 - \delta b_2 - \delta b_3 - \delta b_4$, $\hat{b}_2 = b_2 + \frac{-c_3\delta b_3 - \delta b_4}{2\gamma}$, $\hat{b}_3 = b_3 + \delta b_3$ and $\hat{b}_4 = \gamma + \delta b_4$. The third-order scheme of Table 2 has a fourth-order error estimator if $c_3 = \frac{18}{13}\gamma^2 - 2\gamma + \frac{14}{13}$ using the following expressions for the weights $\hat{b}_1 = \frac{12\gamma c_3 - 4\gamma - 2c_3 + 1}{24\gamma c_3}$, $\hat{b}_2 = \frac{2c_3 - 1}{24\gamma(2\gamma - c_3)(2\gamma - 1)}$, $\hat{b}_3 = \frac{1 - 4\gamma}{12c_3(2\gamma - c_3)(c_3 - 1)}$ and $\hat{b}_4 = \frac{3 + 12\gamma c_3 - 4c_3 - 8\gamma}{12(2\gamma - 1)(c_3 - 1)}$. Stiffly accurate embedded pairs of ESDIRK methods are constructed in [5] in a slightly different form. There the last two successive stages of the implicit scheme are used either as solution or error estimation. A third-order scheme of this type is given in Table 3, here the second-order scheme is not considered.

Table 3: Kvaerno 32: Four-stage, 3rd-order ESDIRK method with embedded 2nd-order scheme

$$
\begin{array}{c|cccc}
0 & 0 & & & \\
2\gamma & \gamma & \gamma & & \\
1 & \frac{-4\gamma^2 + 6\gamma - 1}{4\gamma} & \frac{-2\gamma + 1}{4\gamma} & \gamma & \\
1 & \frac{6\gamma - 1}{12\gamma} & \frac{-1}{(24\gamma - 12)\gamma} & \frac{-6\gamma^2 + 6\gamma - 1}{6\gamma - 3} & \gamma \\
\hline
& & & &
\end{array}
$$

$\gamma = 0.435866521508$:
$\mathbf{W}^4 = \mathbf{U}^{n+1}$
$\mathbf{W}^3 = \mathbf{U}^{\hat{n}+1}$

A five-stage scheme of this form is given in Table 4 with the Butcher coefficients
$$a_{31} = \frac{144\gamma^5 - 180\gamma^4 + 81\gamma^3 - 15\gamma^2 + \gamma}{(12\gamma^2 - 6\gamma + 1)^2}, \quad a_{32} = \frac{-36\gamma^4 + 39\gamma^3 - 15\gamma^2 + 2\gamma}{(12\gamma^2 - 6\gamma + 1)^2)}, \quad a_{41} = \frac{-144\gamma^5 + 396\gamma^4 - 330\gamma^3 + 117\gamma^2 - 18\gamma + 1}{12\gamma^2(12\gamma^2 - 9\gamma + 2)},$$
$$a_{42} = \frac{72\gamma^4 - 126\gamma^3 + 69\gamma^2 - 15\gamma + 1}{12\gamma^2(3\gamma - 1)}, \quad a_{43} = \frac{(-6\gamma^2 + 6\gamma - 1)(12\gamma^2 - 6\gamma + 1)^2}{12\gamma^2(12\gamma^2 - 9\gamma + 2)(3\gamma - 1)}, \quad a_{51} = \frac{(288\gamma^4 - 312\gamma^3 + 120\gamma^2 - 18\gamma + 1}{48\gamma^2(12\gamma^2 - 9\gamma + 2)},$$
$$a_{52} = \frac{24\gamma^2 - 12\gamma + 1}{48\gamma^2(3\gamma - 1)} \quad a_{53} = \frac{-(12\gamma^2 - 6\gamma + 1)^3}{48\gamma^2(3\gamma - 1)(12\gamma^2 - 9\gamma + 2)(6\gamma^2 - 6\gamma + 1)} \text{ and } a_{54} = \frac{-24\gamma^3 + 36\gamma^2 - 12\gamma + 1}{24\gamma^2 - 24\gamma + 4}.$$

4

Table 4: Kvaerno 43: Five-stage, 4th- or 3rd-order stiffly accurate ESDIRK

c	a_{i1}	a_{i2}	a_{i3}	a_{i4}	a_{i5}
0	0				
2γ	γ	γ			
$a_{31}+a_{32}+\gamma$	a_{31}	a_{32}	γ		
1	a_{41}	a_{42}	a_{43}	γ	
1	a_{51}	a_{52}	a_{53}	a_{54}	γ

4th-order
$\gamma = 0.5728160625$:
$\mathbf{W}^s = \mathbf{U}^{n+1}$
$\mathbf{W}^{s-1} = \mathbf{\hat{U}}^{n+1}$
3-rd order
$\gamma = 0.4358665215$:
$\mathbf{W}^{s-1} = \mathbf{U}^{n+1}$
$\mathbf{W}^s = \mathbf{\hat{U}}^{n+1}$

The final scheme, shown in Table 5, is a six-stage, fourth-order stiffly accurate ESDIRK method given by Kennedy, et al. [6].

Table 5: Kennedy 43: Six-stage, 4th-order ESDIRK method with embedded 3rd-order scheme

c						
0	0					
$\frac{1}{2}$	$\frac{1}{4}$	$\frac{1}{4}$				
$\frac{83}{250}$	$\frac{8611}{62500}$	$-\frac{1743}{31250}$	$\frac{1}{4}$			
$\frac{31}{50}$	$\frac{5012029}{34652500}$	$-\frac{654441}{2922500}$	$\frac{174375}{388108}$	$\frac{1}{4}$		
$\frac{17}{20}$	$\frac{15267082809}{155376265600}$	$-\frac{71443401}{120774400}$	$\frac{730878875}{902184768}$	$\frac{2285395}{8070912}$	$\frac{1}{4}$	
1	$\frac{82889}{524892}$	0	$\frac{15625}{83664}$	$\frac{69875}{102672}$	$-\frac{2260}{8211}$	$\frac{1}{4}$
	$\frac{82889}{524892}$	0	$\frac{15625}{83664}$	$\frac{69875}{102672}$	$-\frac{2260}{8211}$	$\frac{1}{4}$
	$\frac{4586570599}{29645900160}$	0	$\frac{178811875}{945068544}$	$\frac{814220225}{1159782912}$	$\frac{-3700637}{11593932}$	$\frac{61727}{225920}$

4 ERROR ESTIMATION AND TIME STEP SIZE CONTROL

The selection of the time step size Δt is performed using an accuracy based controller. For embedded formula pairs with $q = p \pm 1$ time step control can be conducted using I-, PI-, PID- or PC-controllers. Following the basic definition of these controller types according to [6] the coefficients have been adapted for use in TRACE, cf. Eq. 4-7.

$$\Delta t_I^{n+1} \;=\; \rho\,\Delta t^n \left(\frac{TOL}{||\Delta U^{n+1}||_\infty} \right)^{\frac{1}{q}} \tag{4}$$

$$\Delta t_{PI}^{n+1} \;=\; \rho\,\Delta t^n \left(\frac{TOL}{||\Delta U^{n+1}||_\infty} \right)^{\frac{1}{q}} \left(\frac{||\Delta U^n||_\infty}{TOL} \right)^{0.2} \tag{5}$$

$$\Delta t_{PID}^{n+1} \;=\; \rho \, \Delta t^n \left(\frac{TOL}{||\Delta U^{n+1}||_\infty} \right)^{\frac{1}{p}} \left(\frac{||\Delta U^n||_\infty}{TOL} \right)^{\frac{0.45}{p}} \left(\frac{TOL}{||\Delta U^{n-1}||_\infty} \right)^{\frac{0.1}{p}} \tag{6}$$

$$\Delta t_{PC}^{n+1} \;=\; \rho \, \Delta t^n \left(\frac{TOL}{||\Delta U^{n+1}||_\infty} \right)^{\frac{2}{p}} \left(\frac{||\Delta U^n||_\infty}{TOL} \right)^{\frac{1}{p}} \left[\frac{\Delta t^n}{\Delta t^{n-1}} \right] \tag{7}$$

where q is again the accuracy of the solution scheme, p is the accuracy of the error estimator and $\rho = 0.95 - 0.98$ is a constant. The error estimate of the IRK method is defined as

$$\Delta U^{n+1} = U^{n+1} - \hat{U}^{n+1}. \tag{8}$$

Within the context of the present investigation error is measured using the maximum error norm $||\Delta U^{n+1}||_\infty = max(|\Delta U_i^{n+1}|)$.

5 SOLUTION ALGORITHM

To solve the individual stages of the ESDIRK methods a pseudo-time approach is applied. In this approach the pseudo-time term $\partial \mathbf{U}^i / \partial \tau$ is added to each stage of the scheme. Discretizing the pseudo-time term using a first-order approximation and linearizing the residual $\mathbf{R}(\mathbf{U})$ in pseudo-time yields the following linear system of equations

$$\left[\left(\frac{1}{\Delta \tau} + \frac{1}{\Delta t} \right) \mathbf{I} - a_{ii} \frac{\partial \mathbf{R}}{\partial \mathbf{U}} \right] \Delta \mathbf{U} = - \left[\frac{\mathbf{U}^m - \mathbf{U}^n}{\Delta t} - \left(\sum_{j=1}^{i-1} a_{ij} \mathbf{R}(\mathbf{U}^j) + a_{ii} \mathbf{R}(\mathbf{U}^m) \right) \right] \tag{9}$$

where $\mathbf{I}$ is the unity matrix. The solution to stage i is obtained by iterating Eqn. 9 in pseudo-time using a specified number of iterations to drive $\Delta \mathbf{U} \to 0$. With $\Delta \mathbf{U} = 0$, we have $\mathbf{U}^{m+1} = \mathbf{U}^m = \mathbf{U}^i$, and hence the solution $\mathbf{U}^i$ to the i-th stage is obtained. The linear system of equations is solved using the Incomplete Lower Upper ILU(0) method.

6 APPLICATION

6.1 Non-linear stiff ordinary differential equation system

For the basic validation of the embedded error estimators the test problem E4 [7] is used. This is a stiff, non-linear coupled system of ordinary differential equations for which an analytical solution is available. The governing equations are

$$z_1' \;=\; -(\beta_1 z_1 - \beta_2 z_2) + \frac{1}{2}(z_1^2 - z_2^2) \tag{10}$$

$$z_2' \;=\; -(\beta_2 z_1 - \beta_1 z_2) + z_1 z_2 \tag{11}$$

$$z_3' \;=\; -\beta_3 z_3 + z_3^2 \tag{12}$$

$$z_4' \;=\; -\beta_4 z_4 + z_4^2 \tag{13}$$

with

$$z = U^{-1}y \qquad (14)$$

where

$$U = \frac{1}{2}\begin{bmatrix} -1 & 1 & 1 & 1 \\ 1 & -1 & 1 & 1 \\ 1 & 1 & -1 & 1 \\ 1 & 1 & 1 & -1 \end{bmatrix}, \quad \beta = \begin{bmatrix} \beta_1 \\ \beta_2 \\ \beta_3 \\ \beta_4 \end{bmatrix} = \begin{bmatrix} 10 \\ -10 \\ 1000 \\ 0.001 \end{bmatrix}.$$

For the initial conditions $y(0) = (0, -2, -1, -1)^T$ the analytical solution is shown in Fig.1. Using the analytical solution the accuracy of the various error estimators can determined.
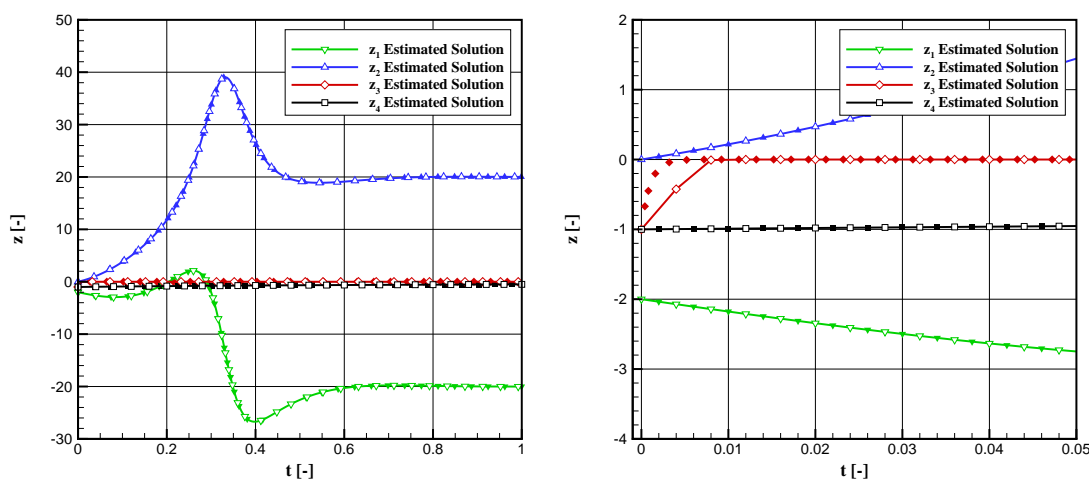
Figure 1: Analytical (symbols) and estimated solution (lines) of E4 problem using a fixed time step size

The results confirm the theoretical order of accuracy of the investigated methods and their embedded schemes Fig. 2 over a wide range of time step sizes. The order of accuracy reduces with decreasing temporal resolution until a certain threshold is reached. Since the third-order methods yield the same error of the solution scheme, only one line is presented in the left figure. Nevertheless it is worth to investigate these schemes, since their error estimation is different, cf. right hand side of Fig. 2. To assess the error estimators, each time step is initialized by the analytical solution. In this way, the exact error deviation from the analytical solution is calculated (symbols in Fig. 3), enabling a comparison to the estimated errors (lines in Fig. 3). A wide spread in the quality of error estimation is observed, ranging from rather bad agreement for the Alexander 32 method (left hand side) to a very good agreement for the Alexander 34 method (right hand side). In other words, the higher order error estimator seems to work much more accurately than the estimator of lower order, a trend which has also been observed for other methods.

7
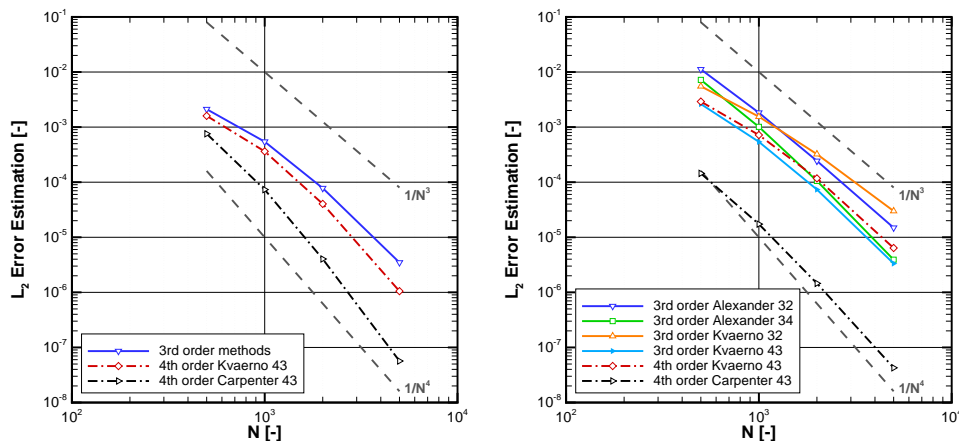
Figure 2: L_2-Error of ESDIRK schemes (left) and of error estimation (right)
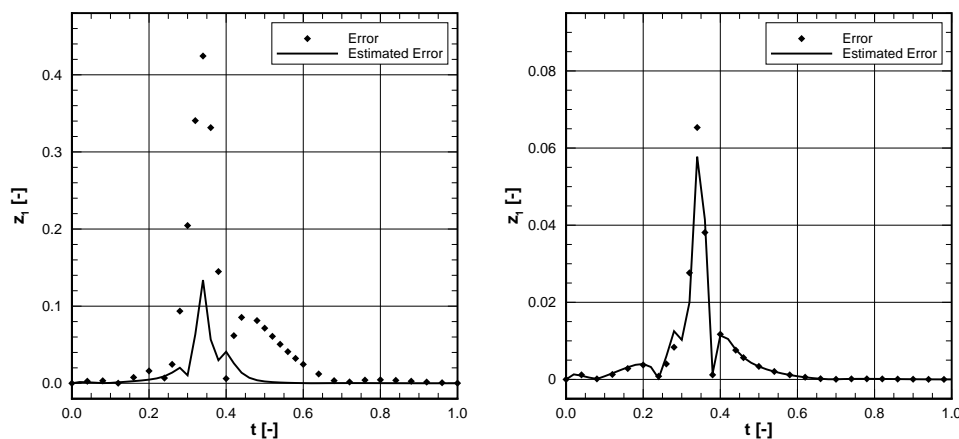
Figure 3: Error estimation compared to analytical error: Alexander 32 (left) and Alexander 34 (right)

6.2 Advection of a two-dimensional entropy disturbance

The second academic test case investigated is the advection of a two-dimensional entropy disturbance in an otherwise uniform subsonic flow. To simulate this problem the compressible Navier-Stokes equations are solved on a uniform, two-dimensional computational domain. The computational domain used in the simulations comprises a simple rectangular block extending $40l$ and $20l$ in the x- and y-directions respectively. The mesh with a total of approximately 12800 cells, split equally over 8 blocks, is used in the simulations. The velocity and pressure fields are uniform and are initialized such that $u = U_\infty$, $v = w = 0$ and $p = P_\infty$. The two-dimensional entropy disturbance is obtained by initializing the density field as follows:

$$\rho = \left[T_\infty - c_3 e^{(1-r^2)} \right]^{\frac{1}{\gamma-1}} \tag{15}$$

where $c_3 = 0.001$, $r = \sqrt{(x - x_0)^2 + (y - y_0)^2}$ and γ is the ratio of specific heats. At $t =$

0 the entropy disturbance is centered about the point $(x_0, y_0) = (10l, 10l)$. The freestream values of axial velocity, pressure and temperature are $U_\infty = 135.6 \, \text{m/s}$, $P_\infty = 90500 \, \text{Pa}$ and $T_\infty = 278.977 \, \text{K}$, respectively. The ability of the applied controller types to closely keep to the prescribed error value is demonstrated by the development of the estimated error L_∞ and the corresponding time step size Δt in Fig. 4. Starting with a large time step size, which also yields a large error, the step size is reduced below the tolerance in only six error checking loops. At this moment, the first unsteady simulation iteration is conducted, and the time step size is subsequently increased, always keeping the estimated error very close to the tolerance. As a representative scheme, Alexander 32 is displayed here. Tests with other ESDIRK schemes (not shown here) show slightly increased distance to the prescribed tolerance, that means to slightly smaller L_∞ values. However, the impact on the time step size and simulation time was not always disadvantageous, as can be seen in the reduced simulation times for some schemes in Tab. 6. As additional information from this table, the third order schemes with second order error estimator (Alexander 32 and Kvaerno 32) yield the best (lowest) simulation times in combination with the P-type controllers. This may not always be a general result, since the controllers have been tuned to this scheme.
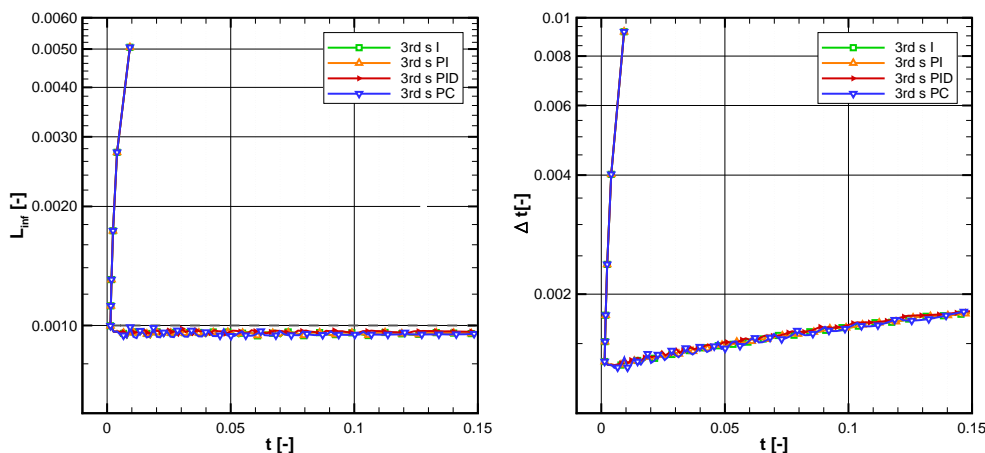
Figure 4: Alexander 32: L_{inf} and Δt

To demonstrate the dynamic adaption capabilities of the controllers, a variable tolerance has also been prescribed for this test case. The tolerance variation is governed by following function:

$$TOL = 0.001 + 0.0008 \cos(20 \cdot 2 \, \pi \, f \, t). \tag{16}$$

The corresponding results in Fig. 5 indicate a reasonable adaption of the estimated error to the prescribed one. The best adaption is achieved with the PC-controller, even for the rejected time steps, which can be recognized by horizontal tolerance displacement in the

9
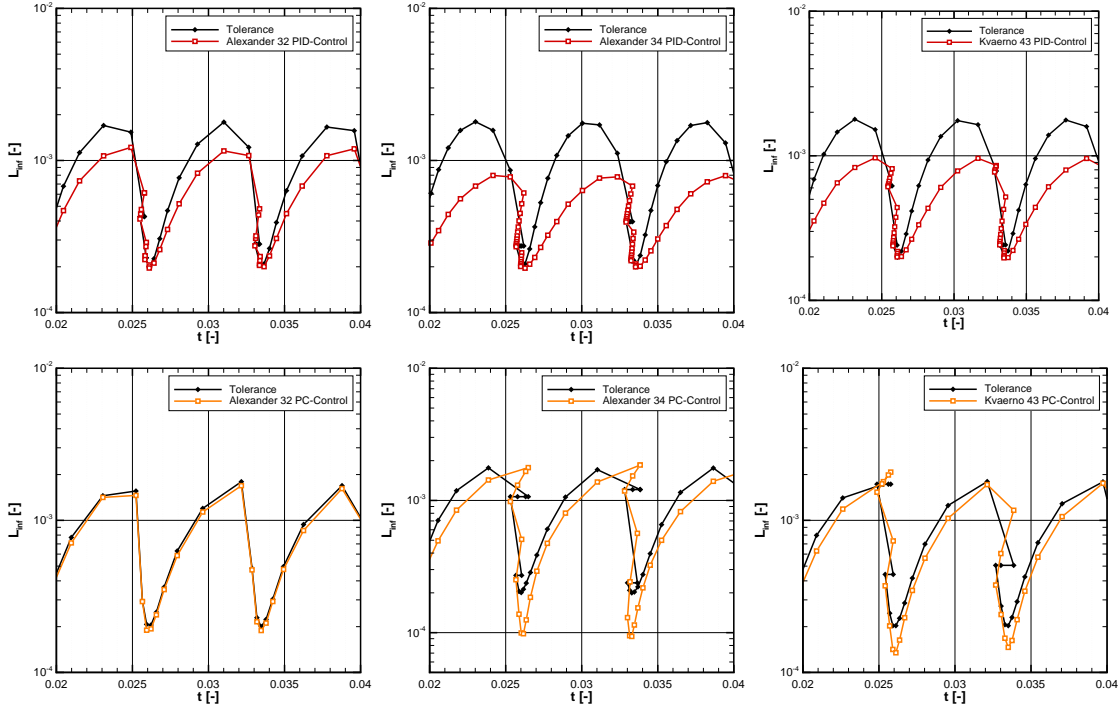
Figure 5: Alexander 32 scheme using variable tolerance and different controller types

left direction. In this case, the PC-controller quickly reduces the time step. Since the other investigated controllers (I, PI and PID) behave very similar, only the PID-controller is presented in this figure. In this case, the adaption is clearly slower.

Table 6: Number of time steps and simulation time for the advection problem with TOL = 0.001 using different controller types

Tol = 0.001		I-Control		PI-Control		PID-Control		PC-Control	
		n_{Steps}	t_{sim}	n_{Steps}	t_{sim}	n_{Steps}	t_{sim}	n_{Steps}	t_{sim}
3rd	Alexander 32	96	120.69	96	79.21	95	78.54	96	86.15
3rd	Alexander 34	96	100.57	96	97.75	101	93.68	107	108.68
3rd	Kvaerno 32	96	92.83	96	76.44	95	80.71	96	66.78
3rd	Kvaerno (4)3	97	145.93	97	143.30	99	144.69	103	133.71
4th	Kvaerno 4(3)	99	119.94	99	126.29	99	128.87	102	122.06
4th	Carpenter	99	194.34	99	183.75	100	178.42	103	182.14

6.3 Flow around a circular cylinder

The last testcase presented in this paper is the flow around a circular with a diameter of 0.10137 m, Reynolds number 140000, free stream velocity of 21.20 m/s and free stream temperature of 24 C. The vortex shedding period is $0.02665s$ (Strouhal number 0.179). Instantaneous eddy viscosity contours from the turbulent cylinder flow simulations are plotted in Fig.6. The simulation results presented here are performed using the third order scheme of Alexander 32 with a given tolerance for the maximal pressure error of 5 Pa (Fig.7). The pressure error level using a fixed time step size $\Delta t = 2.0870e - 04$ (128 time steps per period) oscillates between 10 and 12 Pa (red line, left). With adaptive time stepping conducted with the PI-controller the error is held below the specified tolerance and following the passage of initial transients the time-step size is increased (right).
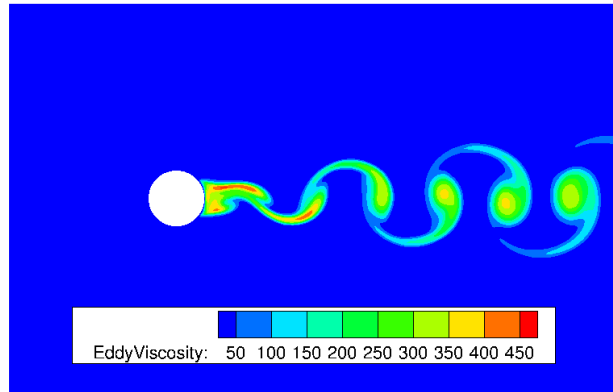
Figure 6: Instantaneous eddy viscosity contours of turbulent cylinder flow
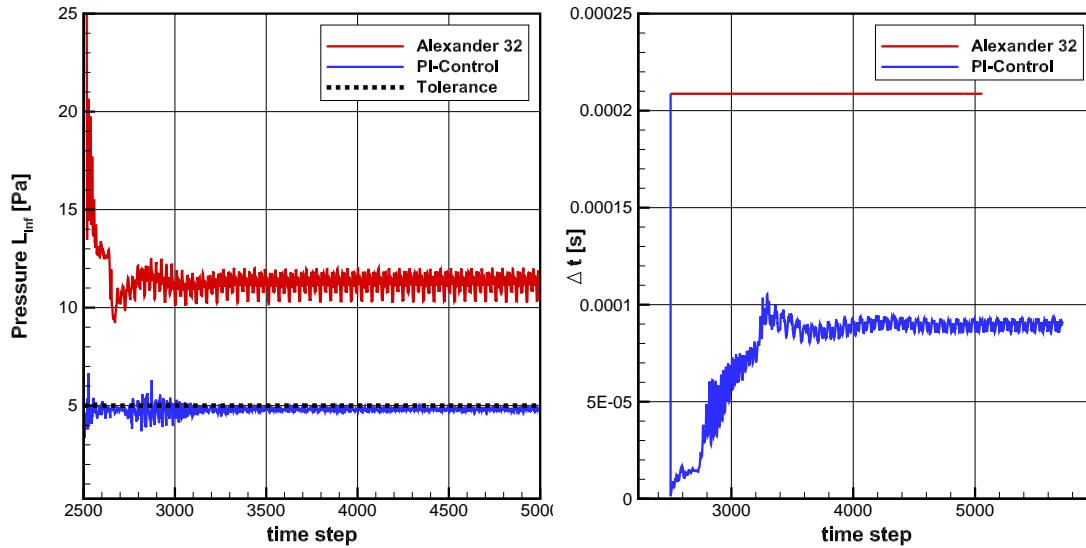
Figure 7: Maximal pressure error and time-step size for cylinder flow

11

7   CONCLUSIONS

Several implicit Runge-Kutta methods with embedded error estimators have been implemented in a compressibly Navier-Stokes solver and applied to a range of test problems.

As a first step to use these methods for error estimation an academic problem has been investigated to show that the proposed embedded schemes are able to estimate the error correctly. Here a wide spread in the quality of the error estimation was observed. In particular, the third-order ESDIRK method Alexander 34 displays excellent error estimation properties.

The ability of the investigated methods to adapt the time step size in order to keep the prescribed tolerance is demonstrated with the second testcase, the advection of entropy disturbance. Both constant and variable tolerances have been prescribed. Here, the PC-controller shows the best properties. Furthermore, the error estimation methods of second order accuracy seem to lead to the shortest simulation times.

As a final test case, the flow around a turbulent cylinder has been analysed. The results demonstrate the ability of the methods in the context of realistic unsteady turbulent flows. The time step size is increased until the prescribed error tolerance is achieved. In this way the simulation accuracy and reliability is considerably improved.

REFERENCES

[1] G. Ashcroft, C. Frey, K. Heitkamp, and C. Weckmüller. Advanced Numerical Methods for the Prediction of Tonal Noise in Turbomachinery - Part I: Implicit Runge-Kutta Schemes. *J. Turbomach.*, 136(2):021003–021003, 2013.

[2] D. Nürnberger and A. Eulitz, F.and Zachcial. Recent Progress in the Numerical Simulation of Unsteady Viscous Multistage Turbomachinery Flow. In *15th International Symposium on Air Breathing Engines, Bangalore, India, Paper n° 2001-1082*, 2001.

[3] E. Kügeler. Numerical Method for the accurate analysis of cooling efficiency in film-cooled turbine-blades. Technical report, Institute of Propulsion Technology, German Aerospace Center, published in German, 2005.

[4] R. Alexander. Design and implementation of DIRK integrators for stiff systems. *Applied Numerical Mathematics*, 46(1):1–17, 2003.

[5] A. Kvaerno. Singly Diagonally Implicit Runge–Kutta Methods with an Explicit First Stage. *BIT Numerical Mathematics*, 44:489–502, 2004.

[6] C. A. Kennedy and M. H. Carpenter. Additive Runge-Kutta Schemes for Convection-Diffusion-Reaction Equations. Technical report, NASA, 2001. NASA/TM-2001-211038.

[7] W. H. Enright, T. E. Hull, and B. Lindberg. Comparing numerical methods for stiff systems of ODEs. *BIT Numerical Mathematics*, 15(1):10–48, 1975.